IOPscience iopscience.iop.org

Home Search Collections Journals About Contact us My IOPscience

One dimensional speckle fields generated by three phase level diffusers

This content has been downloaded from IOPscience. Please scroll down to see the full text.

2015 J. Opt. 17 025602

(http://iopscience.iop.org/2040-8986/17/2/025602)

View the table of contents for this issue, or go to the journal homepage for more

Download details:

IP Address: 137.99.31.134
This content was downloaded on 12/01/2015 at 13:42

Please note that terms and conditions apply.

IOP Publishing Journal of Optics
J. Opt. 17 (2015) 025602 (8pp) doi:10.1088/2040-8978/17/2/025602

One dimensional speckle fields generated by three phase level diffusers

L Cabezas[1], D Amaya[1], N Bolognini[1,2] and A Lencina[1,2]

[1] Centro de Investigaciones Ópticas (CONICET La Plata—CIC), Cno. Centenario y 506, PO Box 3, 1897 Gonnet, Argentina
[2] Departamento de Física, Fac. de Cs. Exactas, Universidad Nacional de La Plata, PO Box 67, 1900 La Plata, Argentina

E-mail: luisac@ciop.unlp.edu.ar (L Cabezas)

Received 23 October 2014, revised 28 November 2014
Accepted for publication 11 December 2014
Published 9 January 2015

Abstract

Speckle patterns have usually been obtained by using ground glass as random diffusers. Liquid-crystal spatial light modulators have opened the possibility of engineering tailored speckle fields obtained from designed diffusers. In this work, one-dimensional Gaussian speckle fields with fully controllable features are generated. By employing a low-cost liquid-crystal spatial light modulator, one-dimensional three phase level diffusers are implemented. These diffusers make it possible to control average intensity distribution and statistical independence among the generated patterns. The average speckle size is governed by an external slit pupil. A theoretical model to describe the generated speckle patterns is developed. Experimental and theoretical results confirming the generation of one-dimensional speckle fields are presented. Some possible applications of these speckles, such as atom trapping and super-resolution imaging, are briefly envisaged.

Keywords: speckle, spatial light modulators, liquid crystal devices
PACS numbers: 42.30.Ms (speckle and moiré patterns), 42.79.Hp (optical processors, correlators, and modulators), 42.79.Kr (display devices, liquid-crystal devices)

(Some figures may appear in colour only in the online journal)

1. Introduction

When a laser beam impinges on a rough surface, the interference produced by the transmitted or reflected light generates random intensity distributions called speckle patterns. The availability of continuous wave lasers since the early 1960s has made the observation of this phenomenon commonplace [1]. The nature of the phenomenon began to be studied, and over the time, different applications were developed, among them those related to optical metrology [2, 3] and optical encryption [4, 5].

It is a common practice to obtain speckle patterns by using ground glass as random diffusers [6, 7]. These diffusers generate 2D random speckles with Gaussian behavior and distinctive second-order statistics according to the structure of the illumination or the pupil of the optical system [8–11]. To the best of our knowledge only applications based on 2D speckle distributions have been developed [12, 13]. These applications have appeared according to the availability of 2D speckle distributions whose features have in fact been determined by the fixed microstructure of the diffuser. Although 1D diffusers exist as commercial products [14] and some research regarding them has been carried out [15–17], they have been studied only in the context of an incoherent optical system, and no investigation regarding speckle generation in 1D has been reported. Regardless of whether speckles are 1D or 2D, it should be emphasized that, to obtain another statistically independent speckle pattern, it is necessary to mechanically displace the diffuser by a certain amount. Similarly, to modify the average intensity distribution it is necessary to replace the diffuser.

To overcome these limitations, real-time programmable features of phase-only liquid crystal spatial light modulators (LC-SLMs) were recently used to generate speckle patterns [18]. In fact, LC-SLMs have opened the possibility of engineering tailored speckle fields [19]. Nevertheless, the analysis

 © 2015 IOP Publishing Ltd Printed in the UK

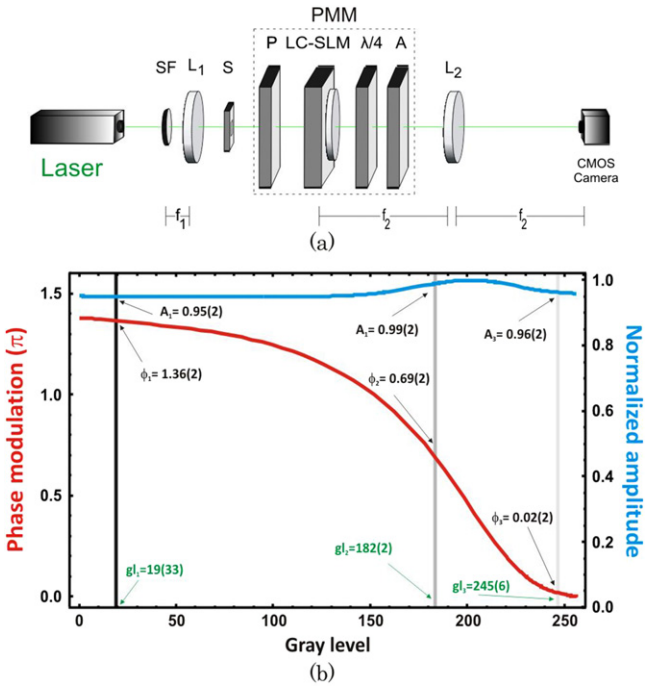

Figure 1. (a) Experimental setup. SF: spatial filter; L_1: collimating lens; L_2: Fourier transforming lens; PMM: phase-mostly modulator composed of P: polarizer, LC-SLM: liquid crystal spatial light modulator, $\lambda/4$: quarter waveplate, and A: analyzer. (b) PMM phase modulation and coupled amplitude response as a function of the gray levels displayed in the LC-SLM. Vertical lines indicate the three gray levels selected to implement the diffusers.

of generated speckles is scarce, and in general, LC-SLMs are employed as black-box tools to generate 2D speckle patterns [20–23]. Although it seems a simple task, several factors limit the quality of the generated speckle. For example, to obtain a Gaussian speckle a uniform random phase distribution in the range 0 to 2π should be sent to the modulator pixels ([7], section 6). Then a phase modulation that does not reach 2π, a phase discretization, a nonlinear phase modulation, system aberrations, an anamorphic response [24, 25], or coupled amplitude could lead to the appearance of a strong zero order or an unwanted non-Gaussian behavior. These points must be dealt with when generating the speckles.

The purpose of this paper is to demonstrate 1D speckle generation without zero order and obeying Gaussian statistics by employing an LC-SLM. In addition it will be shown that a three phase level diffuser suffices to meet this goal, which can be easily accomplished even with a low-cost LC-SLM. In our case we use a transmission LC-SLM (Holoeye LC2002), which has coupled amplitude and a phase modulation that does not reach 2π [26, 27], and which also presents anamorphic behavior [24, 25].

2. Experiment

2.1 Experimental setup

The employed experimental setup is shown in figure 1(a). A laser with a $\lambda = 532$ nm wavelength is filtered and collimated by a spatial filter SF and a lens L_1. The shape of the beam is controlled by a rectangular slit S of fixed height and adjustable width. This beam impinges on a phase-mostly modulator (PMM) composed of a polarizer P, an LC-SLM, a quarter waveplate $\lambda/4$, and an analyzer A. The resulting modulated beam is Fourier transformed by a lens L_2 with focal length $f_2 = 815$ mm and observed by a CMOS DCC1545M Thorlabs camera with 1280×1024 square pixels $5.2\,\mu$m on a side.

2.2 Phase-mostly modulator characterization

After proper orientation of the polarizer, the quarter waveplate, and the analyzer angles is set, the first step is to determine the PMM response. To measure the coupled amplitude the slit S is removed and the camera is placed close to the lens L_2 so that the resultant incident intensity is uniform across its sensor. By projecting uniform gray-level images onto the LC-SLM the coupled amplitude is obtained from the square root of the measured intensity. By averaging over all the pixels, the error of the average amplitude was less than 1%. To measure the phase delay the slit S is replaced by a double aperture pupil and an image is sent to the LC-SLM so that one gray level is fixed in one aperture whereas in the other it is varied. A 10x microscope objective projects the resulting Young pattern interference onto the entire sensor area. From a Fourier analysis of the recorded images the phase delay is determined [27]. Fifty measurements, statistically processed, made it possible to achieve an average phase delay error of less than 1%. The amplitude and phase responses of the PMM are shown in figure 1(b). A maximum phase delay of around 1.38π with a 5% coupled amplitude was obtained.

2.3 Diffuser design

As can be observed in figure 1(b), our PMM does not fulfill the necessary requirements to obtain a Gaussian speckle without zero order: a phase-only response evenly spanned over the interval 0 to 2π. Nevertheless, as is shown hereafter, a Gaussian speckle can still be obtained with this PMM by implementing a phase-discrete diffuser through smart selection of phase levels: three almost equally spaced phases between 0 and 2π with almost the same amplitude. It is important to emphasize that because each of the selected phases distributes one-third of the incident energy, its phasor sum must be as close to zero as possible. To optimize the correct phase selection we search for the minimum of the following estimator:

$$E = \left| \sum_{i=1}^{3} e^{i\varnothing_i} \left(1 - A_i\right) \right|^2$$

where A_i and ϕ_i are the coupled amplitude and the phase imprinted on the field by each macro-pixel taken from the experimental PMM response. Note that this estimator is proportional to the zero order being replaced: $A_q \rightarrow \left(1 - A_q\right)$. In this way, it minimizes the zero order but

searches for high-amplitude levels. At the same time, because the three levels that minimize the estimator are almost equally spaced, this search maximizes the diffraction efficiency [28, section 7.3; 29]. The 'differential evolution' method included in the *NMinimize* built-in function of Mathematica 9 was employed. It found three gray levels (NG1:19, NG2:182, and NG3:245) which minimize the estimator E (see figure 1(b)).

As is well known most LC-SLMs present anamorphic behavior as a function of spatial frequency [24, 25]. However, it is also known that this phenomenon manifests mainly in one direction. Therefore, by implementing Ronchi gratings in our PMM, a frequency analysis was performed and it was verified that one direction of our LC-SLM presented an isomorphic response. This direction was selected to develop the 1D diffusers.

The diffusers were generated with the aim of digitally controlling average intensity distribution and statistical independence among the generated patterns. The latter was managed through the statistical distribution of the three phase levels displayed by the LC-SLM. The former was determined by the lateral 'roughness' of the implemented diffuser. This lateral roughness was controlled through a *macro-pixel*: a number of adjacent single rows of pixels that share the same gray level. Additionally, the transversal speckle size was varied by means of the width of the slit S.

3. A theoretical model for 1D speckles

In this section a model to describe the one-dimensional speckle patterns generated by three phase level diffusers is developed. To begin, the field at the LC-SLM U_0 is described as

$$U_0(\xi,\eta)=\sum_{q=1}^{N}U_{Mpix}\left(\xi-M\,p_p q\right)A_q e^{i\phi_q} rect\left(\frac{\eta}{h_S}\right), \quad (1)$$

where rect(x) is the rectangle function, h_S is the height of the slit S, A_q and ϕ_q are the coupled amplitude and phase imprinted on the field by each macro-pixel, $p_p = 32\,\mu m$ is the LC-SLM pixel pitch, and M is the number of pixel columns included in one macro-pixel. The number of macro-pixels contributing to the field is given by $N = \text{ceil}\left(w_S/M\,p_p\right)$, where w_S is the width of the slit S and ceil(x) is a function that takes the nearest integer higher than x. U_{Mpix} is the function that describes a macro-pixel and is given by

$$U_{\text{Mpix}}(\xi)=f_f\ \text{rect}\left(\frac{\xi}{M\,p_p}\right)\times\left[1+2\sum_{n=1}^{\infty}\text{sinc}\left(\pi f_f n\right)\cos\left(\frac{2\pi n}{p_p}\xi\right)\right], \quad (2)$$

where $f_f = 2/3$ is the LC-SLM fill factor. It follows that the intensity at the Fourier plane of the lens L_2 can be expressed as the Fourier transform of the field U_0, which gives the following result:

$$I=\frac{1}{\left(\lambda f_2\right)^2}\mathcal{F}\left[\text{rect}\left(\frac{\eta}{h_S}\right)\right]^2\mathcal{F}\left[U_{\text{Mpix}}(\xi)\right]^2\times\left[\sum_{q=1}^{N}A_q^2+2\sum_{q=2}^{N}\sum_{r=1}^{q-1}A_qA_r\times\cos\left(\phi_q-\phi_r+\frac{2\pi x}{\lambda f_2}MP_P(q-r)\right)\right], \quad (3)$$

where $\mathcal{F}[x]$ is the Fourier transform operator.

The coupled amplitude A_q and phase ϕ_q of each macro-pixel are uniformly distributed over the three gray levels selected to implement the diffuser, in our case $\left|\left\langle A_q e^{i\phi_q}\right\rangle\right| < 0.004$, which is at the limit of detection of our 8-bit CMOS camera sensor.

Given the foregoing considerations, it is easy to demonstrate that the average intensity distribution at the Fourier plane of the lens L_2 is given by

$$\langle I\rangle=\frac{N\left\langle A_q^2\right\rangle}{\left(\lambda f_2\right)^2}\mathcal{F}\left[\text{rect}\left(\frac{\eta}{h_S}\right)\right]^2\mathcal{F}\left[U_{\text{Mpix}}(\xi)\right]^2. \quad (4)$$

From this model the first- and second-order statistics can be obtained by simulating a large number of speckle patterns.

4. Methods

To verify the feasibility of 1D speckle generation through the PMM, several combinations of the variable slit width ((3.1 ± 0.2) mm, (5.0 ± 0.4) mm, and (7.1 ± 0.8) mm) and the macro-pixel size (1, 2, and 4 pixels) were implemented. Once a three discretized phase levels diffuser was implemented in the PMM, care was taken to ensure that any camera pixel was saturated in the registered patterns and that the transversal speckle sizes were larger than $8/\pi$ camera pixels [30].

To characterize the registered patterns a statistical analysis was performed due to the random nature of the speckle pattern. A Gaussian speckle is characterized by its intensity probability density function, which exhibits a decreasing exponential behavior (first-order statistics), and by its intensity autocorrelation function, which presents a narrow peak (second-order statistics).

To experimentally evaluate the first- and second-order statistics and the average intensity distribution, 1000 statistically independent diffusers were displayed on the PMM and registered by the CMOS camera. Each diffuser was generated by using the *rand* built-in function of the Matlab R2011b software, which is based on the Mersenne twister pseudo-random number generator [31].

The experimental probability density functions of the total intensity were obtained by averaging the histograms from the central region ($x \sim 0$ and $y \sim 0$) of each speckle pattern. The average intensity distributions were achieved by averaging the 1000 recorded speckle patterns. The average

intensity autocorrelations were calculated from the inverse Fourier transform of the squared modulus of the Fourier transform of the recorded intensity and averaged over the 1000 patterns.

For the simulations based on the theoretical model of section 3, statistical distributions of A_q and ϕ_q were generated. To this end, the Mersenne twister pseudo-random number generator [31] of the *RamdomInteger* built-in function of Mathematica 9 was employed. The probability density functions of the total intensity were obtained by averaging 1000 histograms obtained from a central region ($x \sim 0$ and $y \sim 0$) of each simulated speckle pattern. The autocorrelations were obtained from 1000 simulated patterns in the same way as in the experimental case.

5. Results

A summary of our results is depicted in figure 2. For each column both the width of the slit S and the size of the macro-pixel M increase from left to right. Each row shows one of the recorded speckle patterns, the first-order statistics, and the second-order statistics, respectively.

From figures 2(a)–(c) it is noticeable that the random behavior manifests in only one direction, whereas in the perpendicular direction there is no intensity variation except for that corresponding to the diffraction modulation governed by the height of the rectangular slit. Note that in the direction of randomness these 1D speckle patterns have some features that resemble those belonging to 2D results: the speckle size decreases to the extent that the width of the slit increases (see intensity profiles of figures 2(a)–(c)), and the average intensity distribution varies in accordance with the diffraction pattern corresponding to one macro-pixel, i.e., the lateral roughness of the diffuser controls the average intensity distribution.

From the results of figures 2(a)–(c) it is apparent that the use of the PMM enables easy generation of 1D speckle patterns with fully controllable features which are not trivial to produce with only one ground-glass diffuser. It should be noted that the macro-pixel size variation makes it possible to reliably control the lateral roughness of the diffuser, whereas for a physical diffuser there is no alternative but to replace it with another one. Concerning the local distribution of the scattering elements, a new diffuser can be generated as fast as the LC-SLM is refreshed without any mechanical displacement in the experimental setup.

In figures 2(d)–(f) the probability density function of the total intensity of the experimental and simulated speckle and the Gaussian speckle fit are displayed. It is observed that all the experimental histograms exhibit a decreasing exponential behavior which indicates that these speckles satisfy Gaussian statistics. This assertion can be maintained despite the low-intensity points that deviate from the exponential behavior; this issue is analyzed in detail hereafter.

Figures 2(g)–(i) show the experimental and simulated results of the averaged intensity autocorrelation. They present sharp autocorrelation peaks, which indicate a slight lack of correlation between different points in the pattern. As is well known, the peak width provides information about the average transversal speckle size. As can be observed, the peak width diminishes from figure 2(g) to figure 2(i) as the slit width increases. In addition, the background curvature of the autocorrelation increases as the macro-pixel increases. These features are analyzed in detail in the next section.

6. Discussion

6.1 First-order statistics

As is well known a linearly polarized Gaussian speckle presents a negative exponential in the probability density function of the intensity. This function monotonically decreases as the intensity increases. However, as can be seen from figures 2(d)–(f), there are a couple of experimental points, for low-intensity values, that are non-monotonic. By recalling that our diffuser was designed to fulfill the requirements for generating a Gaussian speckle, this behavior could have different sources: depolarization, subsampling, or a coherent background. The latter two sources are discarded because no coherent background with an intensity comparable to the average intensity distribution of the speckle background was involved in the experiment ([1] subsection 2.4.2) and care was taken to ensure that the speckle size was larger than $8/\pi$ camera pixels [30]. Thus depolarization is assumed. This effect is described by the superposition of two uncorrelated speckle patterns on an intensity basis ([7] subsection 3.4), and the expression for the probability density function of the intensity is

$$p_I(I) = \frac{1}{\mathscr{P}\,\bar{I}}\left[e^{-\frac{2}{1+\mathscr{P}}\frac{I}{\bar{I}}} - e^{-\frac{2}{1-\mathscr{P}}\frac{I}{\bar{I}}}\right], \tag{5}$$

where $\mathscr{P}$ is the degree of polarization and $\bar{I}$ is the mean intensity. Under this assumption, by fitting the experimental results (black dots) of figures 2(d)–(f) to equation (5), adjusted R^2 of around 0.98 are obtained. These fits are displayed in figures 2(d)–(f) as green lines. From the adjusted parameters an average degree of polarization of $(86 \pm 2)\%$ is obtained, which is in accordance with reported values [32]. Based on the theoretical model of section 3 and employing the adjusted parameters, it is possible to simulate speckle patterns with these features. The resultant probability density functions are also shown in figures 2(d)–(f) (red dots). From these results it is apparent that the experimentally generated speckles are well described by Gaussian statistics for partially polarized speckles and that the theoretical model statistically reproduces the experimental probability density function of the intensity.

6.2 Average intensity distribution

From equation (4) it can be seen that the average intensity variation along the direction of randomness is related to the Fourier transform of the macro-pixel. This implies that the mean intensity distribution can be controlled by the macro-

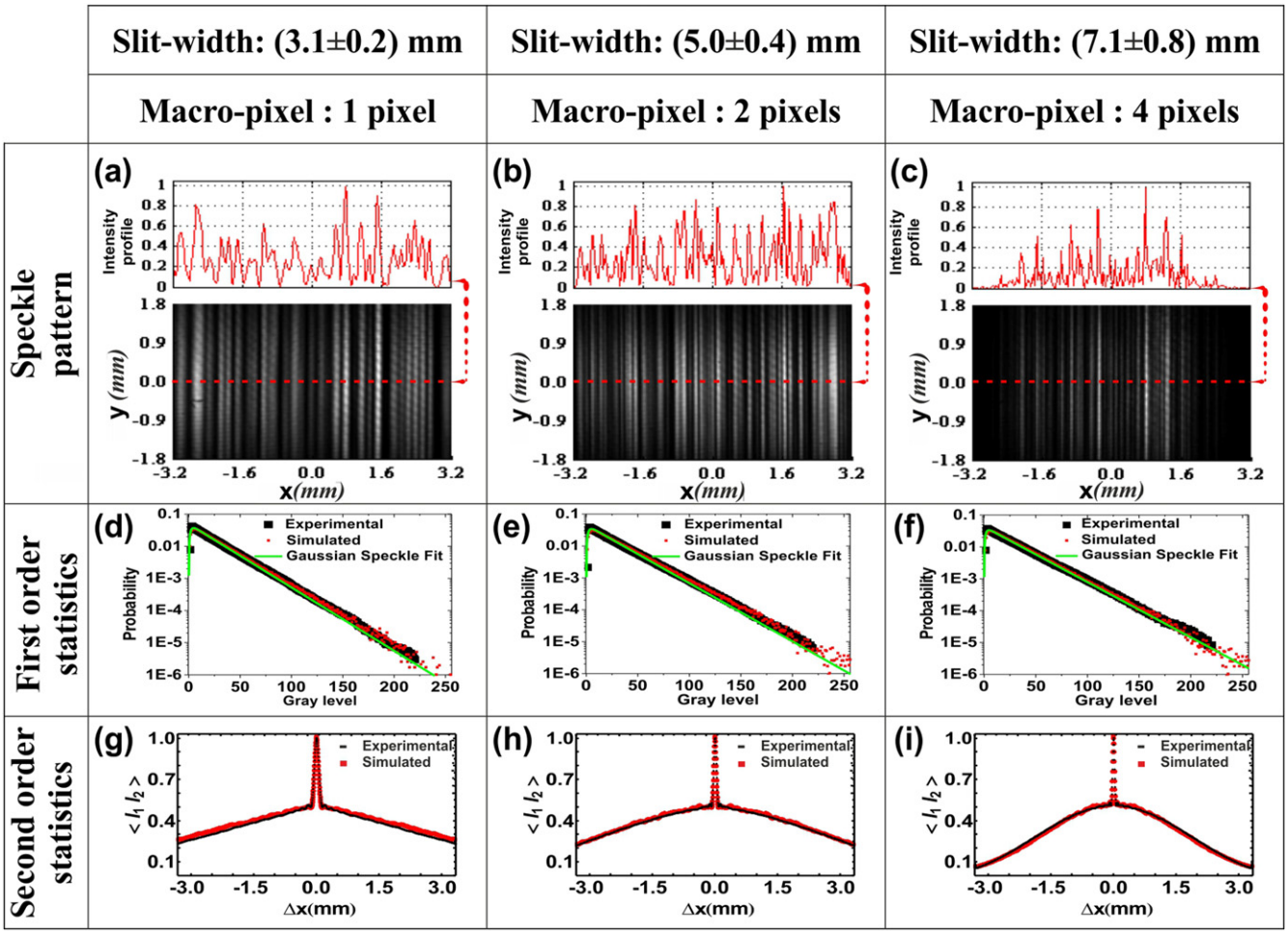

Figure 2. Summary of experimental and simulated results. Each column displays an increasing slit width and macro-pixel size. Rows depict one of the recorded speckle patterns, the probability density function of the total intensity, and the averaged intensity autocorrelation profile, respectively.

pixel size. In order to study this behavior, in figure 3 the profiles along the random direction (for $y = 0$) of the average intensity distribution for the 5.0 mm slit width and different macro-pixels are presented. The dots correspond to experimental results, whereas the continuous lines correspond to plots of equation (4).

From the results is evident that the macro-pixel dominates the width of the averaged intensity distribution: the sharpest and highest shape corresponds to 4 pixels and the flattest one to 1 pixel, whereas the remaining curve has a 2-pixel value. Good agreement between the theoretical plots and the experimental points is observed. It should be stressed that no fitting procedure is performed. These results reinforce the validity of the theoretical model developed in section 3 to describe the 1D speckle patterns generated by three level diffusers in our PMM. The results of this analysis make it clear that the macro-pixel provides a tool to control the average intensity distribution of the generated speckle patterns without changing the second-order statistics. This feature is desired in applications in which increasing the intensity or controlling the bandwidth enhances performance. For example, in optical trapping applications, G Volpe [33] showed that the movement of particles in a static speckle pattern depends on optical forces, which are proportional to the average intensity of the speckle patterns. The particle is virtually freely diffusing when those forces are relatively low. As the forces increase, the particle is metastably trapped in the speckle grains. On the other hand, in optical encryption systems which use diffusers as random phase masks, the

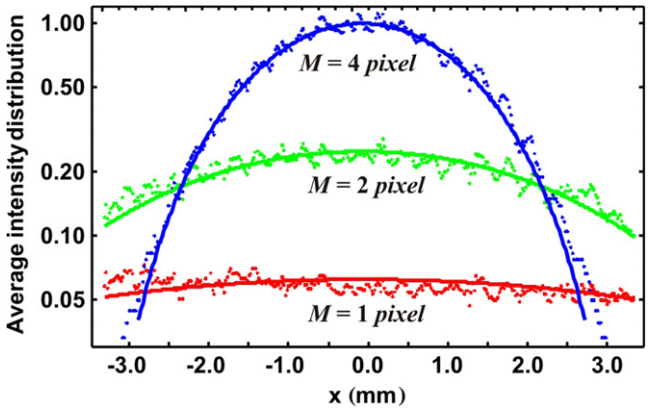

Figure 3. Average intensity distribution for different macro-pixel size values and a slit width of (5.0 ± 0.4) mm.

distribution of information at the output plane is determined by the diffuser roughness [34–36]. Lost information in the recovered image will be avoided if the 'roughness' of the random phase masks is properly adjusted in such a way that all the information is contained in the recorder medium area.

6.3 Averaged intensity autocorrelation

The experimental (black) and simulated (red) autocorrelation (figures 2(g)–(i)) reveal a clear correspondence between them. As is well known, the intensity autocorrelation of the speckle patterns gives information about the speckle size, which is related to the illumination structure incident on the diffuser. But perhaps it is less known that the autocorrelation also contains information about the lateral correlation of the diffuser (generalized van Cittert–Zernike theorem; see reference [7], subsection 4.5.2). This effect is observed in the variation of the autocorrelation function outside the central peak. According to the class of the speckle studied, long-tail correlation peaks, such as those appearing in fractal [9, 23] or clustered speckles [11, 37], could be altered if the macro-pixel is not properly selected. To avoid this, the macro pixel size must be adjusted in such a way as to sufficiently flatten the average intensity so that its influence in modulating the autocorrelation function profile is negligible. However, as previously mentioned, there are certain applications where a flattened autocorrelation background is not necessarily the best choice.

Irrespective of the lateral correlation of the diffuser, for $\Delta x \sim 0$, its contribution can be dismissed and the intensity autocorrelation can be considered stationary [38]. This is an important consideration because it is *there* where the speckle size is measured.

To further analyze the autocorrelation peak structure, the regions around the central peaks of the experimental intensity autocorrelation profiles shown in figures 2(g)–(i) are depicted by dots in figure 4. The inner curve belongs to the 7.1 mm slit width, the outer curve corresponds to the 3.1 mm slit width, and the third curve belongs to the 5.0 mm slit width. The corresponding simulated curves are also displayed as continuous lines. It can be seen that an increase in the slit width produces a decrease in the autocorrelation peak width. It is well known that the width of the central peak at its half-height is proportional to the transversal average speckle size, which, for a rectangular aperture, is given by $(\Delta x)_{1/2} = 0.9\,\lambda\, f_2/w_S$ ([7], subsection 4.4.3). The results of the evaluation of this expression for each slit are represented by arrows inside the central peaks in figure 4. It is evident that this evaluation is in good agreement with the experimental and simulated results.

The results presented confirm the validity of the theoretical model developed in section 3 for simulating the 1D speckle patterns generated by the PMM. At the same time, they are in accordance with the well-known theory of speckles.

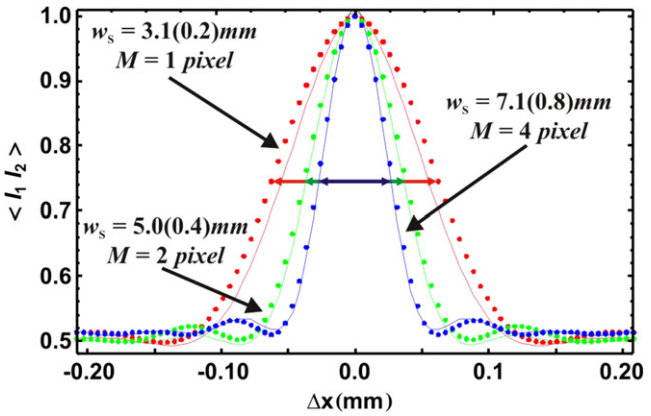

Figure 4. Averaged intensity autocorrelation peaks for the three slit widths and macro-pixel sizes indicated in figure 2.

7. Envisaged applications of 1D speckles

The one-dimensional speckle patterns generated by a PMM may open a new branch of applications where a directional randomness turns out to be of utility to emphasize key aspects of a system. Super-resolution techniques where a sample is illuminated with several random speckle patterns [39, 40] may be evaluated and characterized easily using 1D speckles. Resolution enhancement will manifest only in one direction, whereas in the perpendicular direction a diffraction-limited image for comparison purposes is maintained. On the other hand, there are applications, such as those involving atom trapping [41, 42], which do not require a 2D speckle pattern —in which case 1D patterns may be more appropriate.

8. Conclusions

In this work, one-dimensional speckle fields with controllable features were successfully developed by employing a low-cost phase-mostly modulator as a diffuser. The calibration of this modulator showed a maximum phase delay of 1.38π with a 5% coupled amplitude and anamorphic behavior. Even though these features go against the Gaussianity of speckle patterns, an intelligent implementation of diffusers made it possible to deal with this issue. That is, because the anamorphic behavior manifests mainly in one direction, the 1D diffusers were developed along the isomorphic direction. Moreover, smart selection of the three phase levels distributed almost evenly over the interval 0 to 2π with almost the same amplitude was performed. In addition, this selection precluded the appearance of a zero order. By sending a uniform distribution of the three phase levels to the LC-SLM, a Gaussian speckle was obtained. Statistically independent diffusers were displayed as fast as the LC-SLM could be refreshed. The average intensity distribution was handled by the macro-pixel size of the diffusers. Finally, the transversal speckle size was governed by adjusting the slit width of the setup.

A theoretical model to describe the speckle patterns generated by the one-dimensional three phase level diffusers

implemented in this work was developed. This model enabled simulation of the first- and second-order statistics even with the depolarization introduced by the LC-SLM. Additionally, the average intensity distribution was calculated. The results of this model were in good agreement with the experimental ones.

It should be emphasized that the use of the real-time programmable features of LC-SLMs makes it possible to overcome the limitation of using ground-glass diffusers.

In this work it was demonstrated that a three phase level diffuser suffices to obtain Gaussian speckle fields. The achievements reported in this paper unlock the opportunity to use low-cost LC-SLMs as a reliable tool to obtain one-dimensional Gaussian speckle fields. In the same vein, LC-SLMs with *high-performance* but having a reduced phase modulation for long wavelengths profit from the result of this work.

Future research could focus on the study of the longitudinal intensity autocorrelation of 1D speckles and the control of their transversal intensity autocorrelation via PMM instead of physical apertures. Another issue to study is related to obtaining a uniform intensity distribution with a limited bandwidth; to this end, a tuning of the macro-pixel shape will be required.

Acknowledgments

We acknowledge grants from CONICET PIP 0863 and PIP 0549 and UNLP 11/I168.

References

[1] Dainty J C 1975 *Laser Speckle and Related Phenomena* (Berlin: Springer)
[2] Albertazzi Goncalves A Jr and Kaufmann G H 2010 *Proc. SPIE* **7387**
[3] Kaufmann G H (ed) 2011 *Advances in Speckle Metrology and Related Techniques* (Weinheim: Wiley VCH Verlag) section 6
[4] Amaya D, Tebaldi M, Torroba R and Bolognini N 2009 Wavelength multiplexing encryption using joint transform correlator architecture *Appl. Opt.* **48** 2099–104
[5] Barrera J F, Mira-Agudelo A and Torroba R 2014 Experimental QR code optical encryption: noise-free data recovering *Opt. Lett.* **39** 3074–7
[6] Françon M 1979 *Laser Speckle and Applications in Optics* (New York: Academic Press) section 7
[7] Goodman J W 2007 *Speckle Phenomena in Optics: Theory and Applications* (Colorado: Roberts & Company)
[8] Shirley L G and George N 1989 Speckle from a cascade of two thin diffusers *J. Opt. Soc. Am.* A **6** 765–81
[9] Uozumi J, Kimura H and Asakura T 1991 Laser diffraction by randomized Koch fractals *Waves Random Media* **1** 73–80
[10] O'Donell K A 1982 Speckle statistics of doubly scattered light *J. Opt. Soc. Am.* **72** 1459–63
[11] Lencina A, Staforelli J P, Solano P, Brito J M, Tebaldi M and Bolognini N 2012 Three-dimensional clustered speckle fields: theory, simulations and experimental verification *Opt. Express* **20** 21158
[12] Sirohi R S 1993 *Speckle Metrology* (New York: Marcel Dekker)
[13] Rabal H and Braga R A Jr 2009 *Dynamic Laser Speckle and Applications* (Boca Raton, FL: Taylor & Francis Group)
[14] www.thorlabs.com/thorproduct.cfm?partnumber=ED1-L4100/
[15] Xu X G, Konorov S, Hepburn J W and Milner V 2008 Noise autocorrelation spectroscopy with coherent Raman scattering *Nat. Phys.* **4** 125–1229
[16] Wrzesinski P J, Li H, Harris D A, Xu B, Lozovoy V V and Dantus M 2009 Mode selective single-beam coherent anti-Stokes Raman scattering *Ultrafast Phenomena XVI* (Berlin: Springer-Verlag) 92, 439–41
[17] Präkelt A, Wollenhaupt M, Assion A, Ch H, Sarpe-Tudoran C, Winter M and Baumerta T 2003 Compact, robust, and flexible setup for femtosecond pulse shaping *Rev. Sci. Instrum.* **74** 4950
[18] Cordray J 2010 *Investigation of Liquid Crystal Spatial Light Modulators to Simulate Speckle Fields* (University of Dayton, Ohio)
[19] Bromberg Y and Cao H 2014 Generating non-rayleigh speckles with tailored intensity statistics *Phys. Rev. Lett.* **112** 213904
[20] Dudley A, Vasilyeu R, Belyi V, Khilo N, Ropot P and Forbes A 2000 Controlling the evolution of nondiffracting speckle by complex amplitude modulation on a phase-only spatial light modulator *Opt. Commun.* **182** 95–105
[21] Waller L, Situ G and Fleischer J W 2012 Phase-space measurement and coherence synthesis of optical beams *Nat. Photonics* **6** 474–9
[22] Sun C, Waller L, Dylov D V and Fleischer J W 2012 Spectral dynamics of spatially incoherent modulation instability *Phys. Rev. Lett.* **108** 203902
[23] Funamizu H and Uozumi J 2007 Generation of fractal speckles by means of a spatial light modulator *Opt. Express* **15** 7415
[24] Lizana A, Márquez A, Lobato L, Rodange Y, Moreno I, Iemmi C and Campos J 2010 The minimum Euclidean distance principle applied to improve the modulation diffraction efficiency in digitally controlled spatial light modulators *Opt. Express* **18** 10581
[25] Márquez A, Iemmi C and Moreno I 2005 Anamorphic and spatial frequency dependent phase modulation on liquid crystal displays. optimization of the modulation diffraction efficiency *Opt. Express* **13** 2111
[26] Hermerschmidt A 2009 Experimental modules covering imaging, diffraction, Fourier optics and polarization based on a liquid-crystal cell SLM *Conf. Education and Training in Optics and Photonics (Optical Society of America) EMA6*
[27] Rickenstorff C and Ostrovsky A S 2010 Measurement of the amplitude and phase modulation of a liquid crystal spatial light modulator *Superficies y Vacío* **23** 36–9
[28] Goodman J W 2005 *Introduction to Fourier Optics* (Colorado: Roberts & Company)
[29] Moreno I, Iemmi C, Márquez A, Campos J and Yzuel M J 2004 Modulation light efficiency of diffractive lenses displayed in a restricted phase-mostly modulation display *Appl. Opt.* **43** 6278
[30] Li D, Kelly D P, Kirner R and Sheridan J T 2012 Speckle orientation in paraxial optical systems *Appl. Opt.* **51** A1–10
[31] Matsumoto M and Nishimura T 1998 Mersenne twister: a 623-dimensionally equidistributed uniform pseudo-random number generator *ACM Trans. Model. Comput. Simul.* **8** 3–30
[32] Dev K and Asundi A 2012 Mueller-Stokes polarimetric characterization of transmissive liquid crystal spatial light modulator *Opt. Lasers Eng.* **50** 599–607
[33] Volpe G, Volpe G and Gigan S 2014 Brownian motion in a speckle light field: tunable anomalous diffusion and selective optical manipulation *Scientific Reports* **4** 3936

[34] Nomura T, Nitanal E, Numata T and Javidi B 2006 Design of input phase mask for the space bandwidth of the optical encryption system *Opt Eng*. **45** 17006
[35] Amaya D, Tebaldi M, Torroba R and Bolognini N 2011 Encoding degree testing in a 4f architecture *Proc. SPIE* **8011** 801179
[36] Hennelly B M and Sheridan J T 2005 Optical encryption and the space bandwidth product *Opt. Comm.* **247** 291–305
[37] Lencina A, Tebaldi M, Vaveliuk P and Bolognini N 2007 Dynamic behaviour of speckle cluster formation *Waves in Random and Complex Media* **17** 29–43
[38] Leushacke L and Kirchner M 1990 Three-dimensional correlation coefficient of speckle intensity for rectangular and circular apertures *J. Opt. Soc. Am.* A **7** 827–32
[39] Mudry E, Belkebir K, Girard J, Savatier J, Le Moal E, Nicoletti C, Allain M and Sentenac A 2012 Structured illumination microscopy using unknown speckle patterns *Nat. Photonics* **6** 312–5
[40] Fixler D, Garcia J, Zalevsky J Z, Weiss A and Deutsch M 2007 Speckle random coding for 2D super resolving fluorescent microscopic imaging *Micron* **38** 21–128
[41] Bilas N and Pavloff N 2006 Anderson localization of elementary excitations in a one-dimensional Bose–Einstein condensate *Eur. Phys. J.* D **40** 387–97
[42] Lewenstein M, Sanpera A, Ahufinger V, Damski B, Sen A and Sen U 2007 Ultracold atomic gases in optical lattices: mimicking condensed matter physics and beyond *Adv. Phys.* **56** 243–379